Hyperspectral absorption coefficient of "pure" seawater in the range of 350–550 nm inverted from remote sensing reflectance

Zhongping Lee,[1,*] Jianwei Wei,[1] Ken Voss,[2] Marlon Lewis,[3] Annick Bricaud,[4,5] and Yannick Huot[6]

[1]School for the Environment, University of Massachusetts Boston, Boston, Massachusetts 02125, USA

[2]Department of Physics, University of Miami, Coral Gables, Florida 33124, USA

[3]Department of Oceanography, Dalhousie University, Halifax, Nova Scotia B3H 4J1, Canada

[4]Sorbonne Universités, UPMC Univ Paris 06, UMR 7093, LOV, Observatoire océanologique, F-06230, Villefranche/mer, France

[5]CNRS, UMR 7093, LOV, Observatoire océanologique, F-06230, Villefranche/mer, France

[6]Département de géomatique appliquée, Université de Sherbrooke, Sherbrooke, Quebec J1K 2R1, Canada

*Corresponding author: zhongping.lee@umb.edu

Hyperspectral (every 5 nm) absorption coefficients of "pure" seawater in the range of 350–550 nm are derived from remote sensing reflectance measured in oligotrophic oceans. The absorption spectrum is reduced by ∼50–70% for the 350–400-nm range and ∼5–10% for the 510–530-nm range compared with the commonly adopted standard for ocean color processing and shows different spectral curvatures. The application of this new spectrum resulted in better retrievals of the phytoplankton absorption coefficient in oligotrophic oceans and will provide better closure of remote sensing reflectance for the UV–visible domain.   © 2015 Optical Society of America

OCIS codes: (010.1030) Absorption; (010.4450) Oceanic optics; (010.0280) Remote sensing and sensors; (010.7340) Water.

http://dx.doi.org/10.1364/AO.54.000546

1. Introduction

The spectral absorption coefficient of pure seawater $[a_w(\lambda)\,(\mathrm{m}^{-1})]$ is a basic inherent optical property (IOP) [1]. It is required for estimating and analyzing the light field in the upper ocean and is critical for analytically processing ocean color data. Because of its importance, many $a_w(\lambda)$ data have been obtained and reported in the literature (see reviews in Morel and Prieur [2], Smith and Baker [3], Pope and Fry [4], and Fry [5]). Because of various limita-

tions, including the preparation of a "pure" water sample and the technical challenges associated with measuring very low absorption coefficients and separating them from scattering effects [6], these reported $a_w(\lambda)$ values differ by a factor of up to 5 in the shorter wavelengths, particularly for wavelengths in the range of ∼350–500 nm (see Fig. 1 in Smith and Baker [3] and Fig. 10 in Pope and Fry [4], for instance). For ocean optics studies and ocean color data processing, the values in Pope and Fry [4] [represented as $a_w^{\mathrm{PF}}(\lambda)$ and $a_w^{\mathrm{SPF}}(\lambda)$ after merging the values of Pope and Fry [4] for wavelengths equal to or greater than 380 nm with those of Sogandares and Fry [7] for wavelengths of less than 380 nm] have

been adopted as the "standard" by the ocean color community. However, an application of $a_w^{\mathrm{SPF}}(\lambda)$ when modeling the remote sensing reflectance [$R_{\mathrm{rs}}(\lambda)$ (sr^{-1}), which is the ratio of the water-leaving radiance to the downwelling irradiance just above the surface] of oligotrophic oceans does not produce appropriate spectral curvature for wavelengths of around 400 nm [8]. In addition, for measurements made in the South Pacific Gyre, where the "clearest" natural water [9] has been measured, the application of $a_w^{\mathrm{SPF}}(\lambda)$ will result in negative absorption coefficients of yellow substance for wavelengths of around 420 nm [9]. As further demonstrated in the following sections, measurements in the oligotrophic oceans indicate that values of $a_w^{\mathrm{SPF}}(\lambda)$ in the shorter wavelengths (~350–450 nm) do not provide a closure for $R_{\mathrm{rs}}(\lambda)$ of such waters. As Fry [5] pointed out, "There does not seem to be a best choice of data covering the gap $320\ \mathrm{nm} \le \lambda \le 380\ \mathrm{nm}$." Because NASA and the international community are pushing ocean color remote sensing to the UV region and the 350- to 400-nm spectral window could be significantly important for the retrieval of the absorption coefficient of gelbstoff or yellow substance [10,11], it is thus urgently important to determine an appropriate $a_w(\lambda)$ spectrum for the UV–visible domain. Here, we address this problem through the use of the highest-quality data from oligotrophic oceans, where $a_w(\lambda)$ play a larger role compared with more productive waters and derive an effective $a_w(\lambda)$ from the $R_{\mathrm{rs}}(\lambda)$ spectrum. After demonstrating the nonclosure of $R_{\mathrm{rs}}(\lambda)$ in these waters when applying $a_w^{\mathrm{SPF}}(\lambda)$, details of the specific data and methodologies for the derivation of $a_w(\lambda)$ are presented, followed by the resultant $a_w(\lambda)$. The impact of this $a_w(\lambda)$ on analytical retrievals of the phytoplankton absorption coefficients in oligotrophic waters is then discussed.

2. Motivation

Because $R_{\mathrm{rs}}(\lambda)$ is a function of the IOPs [12,13], the measured $R_{\mathrm{rs}}(\lambda)$ should match the $R_{\mathrm{rs}}(\lambda)$ calculated with the measured IOPs of the same water body if all components are well determined experimentally and if the assumptions of the models are fully met. For the South Pacific Gyre, comprehensive measurements of a wide range of water properties were made during the BIOSOPE cruise [14], which included $R_{\mathrm{rs}}(\lambda)$ [9,15] and various component IOPs [16–18]. To check the closure of $R_{\mathrm{rs}}(\lambda)$, a simplified but widely used relationship between $R_{\mathrm{rs}}(\lambda)$ and the IOPs developed based on numerical simulations of radiative transfer [19] was used

$$r_{\mathrm{rs}}(\lambda) = \left(0.0979 + 0.0794\frac{b_b(\lambda)}{a(\lambda)+b_b(\lambda)}\right)\frac{b_b(\lambda)}{a(\lambda)+b_b(\lambda)}, \tag{1}$$

where $r_{\mathrm{rs}}(\mathrm{sr}^{-1})$ is the subsurface remote sensing reflectance, which is related to the above-surface remote sensing reflectance (R_{rs}) through [19,20]

$$R_{\mathrm{rs}}(\lambda) = \frac{0.52r_{\mathrm{rs}}(\lambda)}{1 - 1.7r_{\mathrm{rs}}(\lambda)}. \tag{2}$$

Here, a and b_b are the total absorption and backscattering coefficients (units in m^{-1}), respectively, and can be expressed as [21,22]

$$a(\lambda) = a_w(\lambda) + a_{\mathrm{ph}}(\lambda) + a_d(\lambda) + a_y(\lambda),$$
$$b_b(\lambda) = b_{bw}(\lambda) + b_{bp}(\lambda). \tag{3}$$

$a_{\mathrm{ph},d,y}$ are the absorption coefficients of the phytoplankton pigments, detritus, and yellow substance, respectively; and b_{bw} and b_{bp} are the backscattering coefficient of pure seawater and the suspended particles, respectively. Generally, the spectra of both a_w and b_{bw} are assumed to be well known and are taken as constants for the global oceans, although they vary slightly with temperature and salinity [23–25]. Therefore, when the values of spectral $a_{\mathrm{ph},d,y}$ and b_{bp}—i.e., the IOPs of the active constituents—are known, it is straightforward to calculate $R_{\mathrm{rs}}(\lambda)$ based on Eqs. (1)–(3). In addition, if both the active IOPs and R_{rs} are accurately determined in the field and Eqs. (1) and (2) are accurate, the modeled R_{rs} with the measured IOPs should match the measured R_{rs}—i.e., a closure in R_{rs} will be achieved.

For measurements made in the South Pacific Gyre during the BIOSOPE cruise, instead of comparing the measured-versus-modeled $R_{\mathrm{rs}}(\lambda)$ station by station, we compared the averaged $R_{\mathrm{rs}}(\lambda)$ of the "clearest" waters (Stations GYR2-5 and STB6-8) with the modeled $R_{\mathrm{rs}}(\lambda)$ using the averaged IOPs as inputs to show a generalized pattern between the measured and modeled $R_{\mathrm{rs}}(\lambda)$. For an easier description of the component IOPs (e.g., $a_{\mathrm{ph},d,y}$ and b_{bp}), their spectral dependences are described following common practice [26,27] as

$$a_{\mathrm{ph}}(\lambda) = a_{\mathrm{ph}}(440)a_{\mathrm{ph}}^{+}(\lambda), \tag{4a}$$

$$a_d(\lambda) = a_d(440)e^{-S_d(\lambda-440)},$$
$$a_y(\lambda) = a_y(440)e^{-S_y(\lambda-440)}, \tag{4b}$$

$$b_{bp}(\lambda) = b_{bp}(550)\left(\frac{550}{\lambda}\right)^{Y}. \tag{4c}$$

Here, $a_{\mathrm{ph}}^{+}(\lambda)$ is the dimensionless spectral shape of $a_{\mathrm{ph}}(\lambda)$ and was obtained from sample measurements [16]. For these super-blue waters, $a_{\mathrm{ph}}(440)$ was found to be ~0.0015 m^{-1}, with an $a_d(440)$ of ~0.0005 m^{-1} and an $a_y(440)$ of ~0.0016 m^{-1} [16]. $S_{d,y}$ (nm^{-1}) and Y are the spectral shape parameters for $a_{d,y}$ and b_{bp}, respectively; S_d was found to be ~0.0094 nm^{-1} and S_y was found to be ~0.0145 nm^{-1} [16]. The averaged $b_{bp}(550)$ for the South Pacific Gyre was measured as ~0.0003 m^{-1} [17,28], but a value of 0.0003 m^{-1} was added to this measurement to reflect a likely uncertainty in the measured b_{bp} [18] and to
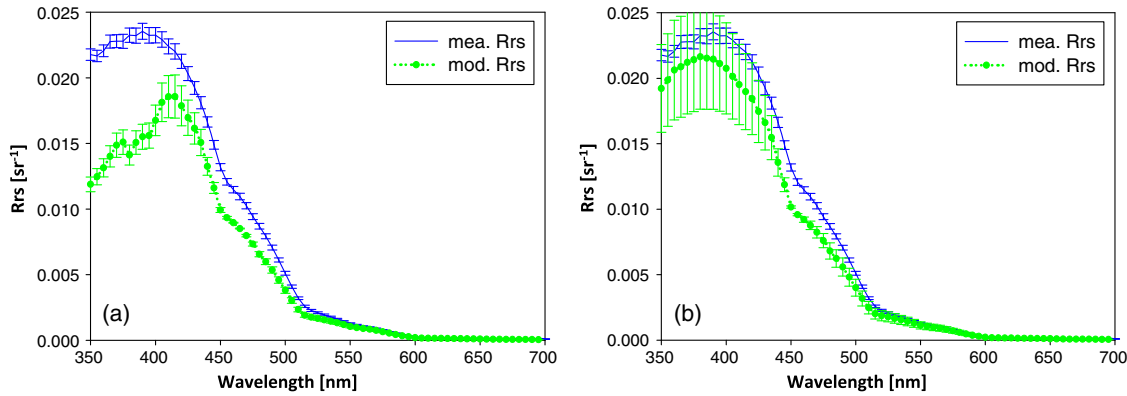
Fig. 1. Comparison between measured (blue) and modeled (green) R_{rs} spectra for measurements made in the South Pacific Gyre (November 2004). Measured R_{rs} represents the average of 12 casts of the "clearest" oceanic waters, and contribution from Raman scattering is removed empirically (refer to Section 4.B). Modeled R_{rs} (Mod_Rrs) is generated [Eqs. (1)–(4)] using the component IOPs measured at the same "clearest" stations by adding ±50% uncertainty to each optically active component. (a) Mod_Rrs used pure water absorption coefficients from Pope and Fry [4] (for wavelengths from 380 to 700 nm) and that from Sogandares and Fry [7] (for wavelengths from 350 to 370 nm). (b) Mod_Rrs used pure water absorption coefficients from Pope and Fry [4] for wavelengths from 420 to 700 nm and those from Boivin [30] for wavelengths from 350 to 420 nm, as proposed by Morel et al. [9].

ensure an R_{rs} closure at 550 nm—i.e., $a_w(550)$ from Pope and Fry [4] was considered correct. The dimensionless exponent Y was taken as 1.9 based on the measured b_{bp} values at 470 and 550 nm [28]. For the modeling of $R_{rs}(\lambda)$ of such super-blue waters, the magnitudes of the component IOPs [e.g., $a_{ph,d,y}(440)$ and $b_{bp}(550)$] were further disturbed by ±50% to show the range of $R_{rs}(\lambda)$ that would be expected with these IOPs. On the other hand, for $a_w(\lambda)$, both $a_w^{SPF}(\lambda)$ and that recommended in Morel et al. [9] (a_{w1}) were used, respectively.

Figure 1(a) shows the range of modeled $R_{rs}(\lambda)$ spectra (green lines) with $a_w^{SPF}(\lambda)$ and the active IOPs described previously, along with the averaged $R_{rs}(\lambda)$ spectrum from 12 measurements of super-blue waters (Stations GYR2-5 and STB6-8), where $R_{rs}(440)/R_{rs}(550)$ is larger than 12.0. Clearly there are large differences between the modeled and the measured $R_{rs}(\lambda)$ in the 350–500-nm range, even with a ±50% range of the measured component IOPs. Not only are the values quite different but also the curvatures do not match each other. In particular, the modeled $R_{rs}(\lambda)$ in the 350–400-nm range are ~40% smaller than the measured $R_{rs}(\lambda)$. In other words, there is no closure in $R_{rs}(\lambda)$ for the 350–500-nm range. It is unlikely that the measured $R_{rs}(\lambda)$ have such large overestimations, as the coefficient of variation at each wavelength of the 12 $R_{rs}(\lambda)$ spectra (measured at seven stations) is less than 4%. Further, the uncertainty of the R_{rs}–IOP model itself [Eq. (1)] is just about 10% [19] (also refer to Section 4.A), which cannot explain the large deviations, specifically in the 350–400-nm window. This nonclosure actually echoes the finding of Morel et al. [9] that the $a_w^{SPF}(\lambda)$ values in the ~350–400-nm range are too high for such waters.

Buiteveld et al. [29] and Morel et al. [9] proposed using spectrally interpolated $a_w(\lambda)$ from the discrete measurements in the UV in Boivin et al. [30] for values in the shorter wavelengths, and Morel et al. [9]

suggested linking Boivin et al. [30] $a_w(\lambda)$ data after interpolation with that measured by Pope and Fry [4] at 420 nm [represented as $a_w^{MPF}(\lambda)$ in the following]. Thus, with the same IOPs but replacing the $a_w^{SPF}(\lambda)$ values with those of $a_w^{MPF}(\lambda)$, the modeled $R_{rs}(\lambda)$ are compared with the $R_{rs}(\lambda)$ of the super-blue waters again [refer to Fig. 1(b)]. For the same range of the component IOPs, the closure of $R_{rs}(\lambda)$ for wavelengths in the range of ~350–410 nm improved significantly, but there was no improvement for wavelengths of around 450 nm [the modeled $R_{rs}(\lambda)$ was still ~20% less than the measured $R_{rs}(\lambda)$]—a spectral window important for analytical derivation of the absorption coefficients of phytoplankton and yellow substance. These observations support the findings of earlier studies regarding the nonsuitability of the current "standard" pure water absorption coefficients in the shorter wavelengths. In short, because (1) the results of Boivin et al. [30] are associated with large uncertainties [4]; (2) the combination of the values of Biovin et al. [30] and those of Pope and Fry [4] is subjective; and (3) the merger provides only "an upper limit of pure water absorption coefficient" [9], it is thus important and necessary to obtain an $a_w(\lambda)$ spectrum that is consistent with field observations.

3. Data

Data used for the derivation of $a_w(\lambda)$ spectral values were collected in the South Pacific Gyre and at the Marine Optical Buoy (MOBY). During the BIOSOPE cruise (November 2004), a free-fall hyperspectral (350–800 nm, 10-nm bandwidth, 3-nm interval) radiometer (Satlantic, Inc.) was used to measure the vertical profiles of upwelling radiance and downwelling irradiance for a series of stations located in the Southeast Pacific Ocean [14]. Remote sensing reflectance (R_{rs}) was calculated from these profiles. Details of the data processing can be found in Lee et al. [15]. Figure 2(a) presents examples of $R_{rs}(\lambda)$ from these

measurements, with $R_{rs}(\lambda)$ of pure seawater [simulated with HydroLight [31] and $a_w^{SPF}(\lambda)$ for absorption coefficients of pure seawater] also included, which shows that the $R_{rs}(\lambda)$ values of pure seawater are lower than those of the "clearest" natural water for the range of ~350–400 nm.

During the BIOSOPE cruise, there were also extensive measurements of the absorption coefficients of phytoplankton pigments, yellow substance, and the scattering and backscattering coefficients of particles (see Bricaud et al. [16], Twardowski et al. [17], and Stramski et al. [18]). Data of these measurements can be accessed at http://www.obs-vlfr.fr/proof/vt/op/ec/biosope/bio.htm.

MOBY [32] is located approximately 20 km west of Lanai, Hawaii, where hyperspectral (~1.0 nm resolution) measurements of upwelling radiance are made at 1, 5, and 9 m below the surface, and water-leaving radiance was estimated from these measurements [32]. An irradiance sensor is placed above the surface to measure downwelling irradiance just above the surface for the calculation of $R_{rs}(\lambda)$. For this study, to have an adequate representation, three days of high-quality $R_{rs}(\lambda)$ for each season in 2013 were randomly acquired from the MOBY website http://coastwatch.noaa.gov/data/moby/filtered_spec/. For each day, two $R_{rs}(\lambda)$ spectra (calculated from the upwelling measurements of the 1- and 5-m arms) were used, resulting in a total of 24 $R_{rs}(\lambda)$ from the MOBY measurements utilized for this study. Figure 2(b) presents examples of MOBY $R_{rs}(\lambda)$ (binned to 5-nm bandwidth and interpolated to 5-nm resolution), where the highest values are approximately 0.016 sr^{-1}, whereas the highest values for the South Pacific Gyre are approximately 0.025 sr^{-1}. This is expected because the South Pacific Gyre is considered the most oligotrophic area of the world's oceans; thus, the absorption coefficients of MOBY waters (not measured) are expected to be higher. The bumps in the MOBY $R_{rs}(\lambda)$ around 400 nm—not highly visible in the BIOSOPE data because of the lower spectral resolution—are the results of the filling of the Fraunhofer line [33] in the upwelling radiance from Raman scattering.

4. Method

A. Model for Remote Sensing Reflectance

The analytical derivation of bulk IOPs—and subsequently, $a_w(\lambda)$—uses the dependence of $R_{rs}(\lambda)$ as a function of the IOPs, along with the measured $R_{rs}(\lambda)$ as inputs. Decades of numerical simulations of radiative transfer have resulted in many analytical forms to describe the relationship between $R_{rs}(\lambda)$ and the bulk IOPs, specifically $a(\lambda)$ and $b_b(\lambda)$ [19,34,35]. Using the most "accurate" model to obtain $a(\lambda)$ from $R_{rs}(\lambda)$ is important, as a modeling error in $R_{rs}(\lambda)$ will be propagated to the inverted $a(\lambda)$ and then $a_w(\lambda)$. The relationship widely used by the community was developed by Gordon et al. [19]—i.e., Eq. (1). In this relationship, the spectral change of the scattering phase function of the bulk water is ignored [36,37]. As a result, independent of wavelength, the estimated $r_{rs}(\lambda)$ will be the same as long as the ratio $b_b(\lambda)/[a(\lambda) + b_b(\lambda)]$ is the same. The same approach was followed for a fourth-order polynomial function developed by Albert and Mobley [38], leading to the same wavelength-independent behavior, where $r_{rs}(\lambda)$ is described as

$$r_{rs}(\lambda) = \omega \sum_{i=1}^{4} \left(g_i \frac{b_b(\lambda)}{a(\lambda) + b_b(\lambda)} \right)^i, \qquad (5)$$

with parameter ω describing the effects due to wind speed and sun sensor viewing geometry and g_1 (sr^{-1}) for modeling coefficients to fit numerically simulated $r_{rs}(\lambda)$.

However, water molecular scattering (Rayleigh scattering) is much stronger at shorter wavelengths than at longer wavelengths [39], and its scattering phase function is markedly different from that of particle scattering. Therefore, it is necessary to separate the effects of molecular and particle scatterings in the resulting solution [40,41]. One attempt is the model developed by Lee et al. [36], where the two scattering processes are separated explicitly in an $r_{rs}(\lambda)$ model:
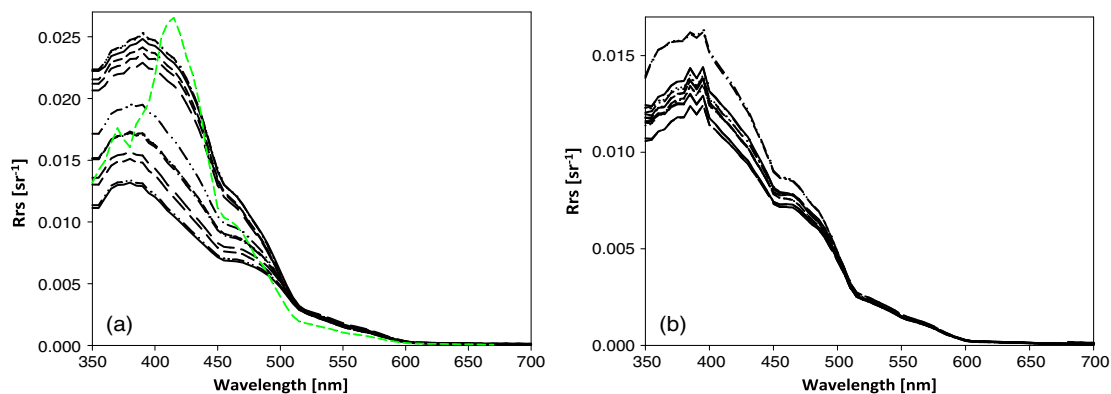

Fig. 2. Remote sensing reflectance measured at (a) South Pacific Gyre and (b) the MOBY. $R_{rs}(\lambda)$ of pure seawater, simulated by HydroLight with $a_w^{SPF}(\lambda)$ for pure water absorption coefficients, is included in (a) (green line) for a visual comparison.

$$r_{rs}(\lambda) = 0.113 \frac{b_{bw}(\lambda)}{a(\lambda) + b_b(\lambda)} + g_p \frac{b_{bp}(\lambda)}{a(\lambda) + b_b(\lambda)}, \quad (6)$$

with model parameter $g_p (\mathrm{sr}^{-1})$ described as

$$g_p = 0.197 \left[1 - 0.636 \exp \left(-2.552 \frac{b_{bp}(\lambda)}{a(\lambda) + b_b(\lambda)} \right) \right]. \quad (7)$$

Because the g_p function is complex, b_{bp} cannot be solved analytically from the known r_{rs} and a as processed in the quasi-analytical algorithm (QAA) [20], and thus data processing efficiency is reduced. To remedy this efficiency limitation, Eq. (6) and the transmission function [Eq. (2)] were bundled together as in Park and Ruddick [37] and modeled as [42]

$$R_{rs}(\lambda) = \left(G_0^w + G_1^w \frac{b_{bw}(\lambda)}{a(\lambda) + b_b(\lambda)} \right) \frac{b_{bw}(\lambda)}{a(\lambda) + b_b(\lambda)}$$
$$+ \left(G_0^p + G_1^p \frac{b_{bp}(\lambda)}{a(\lambda) + b_b(\lambda)} \right) \frac{b_{bp}(\lambda)}{a(\lambda) + b_b(\lambda)}, \quad (8)$$

with the model parameters $(G_0^w, G_1^w, G_0^p, G_1^p)$ for various sun sensor viewing geometries determined through HydroLight simulations [42].

To account for the change of the scattering phase function for different particle loading, Park and Ruddick [37] also employed a fourth-order polynomial function of $b_b(\lambda)/[a(\lambda) + b_b(\lambda)]$ to model $R_{rs}(\lambda)$ but introduced b_{bp}/b_b-dependent $g_i (\mathrm{sr}^{-1})$ coefficients, with values of g_i tabulated for eight b_{bp}/b_b ratios. Because it is not straightforward to describe the wavelength dependence of these model parameters, a comparison with this model is omitted herein. Also omitted for comparison is the model developed by Morel and Gentili [43] and Morel et al. [44], where r_{rs} is described as a function of $g * b_b/a$, with g (which is termed f/Q [44]) values tabulated for six chlorophyll concentrations, seven wavelengths, and a series of sun sensor angles under the assumption of "Case 1" bio-optical dependences [45]. Because the data under study are hyperspectral, this r_{rs} model is thus not straightforwardly applicable.

To evaluate how the aforementioned analytical models perform for oligotrophic waters, five $R_{rs}(\lambda)$ spectra for the wavelength range of 350–700 nm (5-nm resolution) and chlorophyll concentrations ([Chl]) of 0.02, 0.05, 0.1, 0.2, and 0.5 mg/m^3 were simulated with HydroLight (V. 5.1.2) [31]. In these simulations, the sun angle was set as 30° from zenith, with default bio-optical models embedded in HydroLight for the component IOPs, except that the factor (F) for the yellow substance absorption coefficient at 440 nm was set as 1.0 [i.e., $a_y(440) = a_{ph}(440)$] for all five [Chl] values to better represent oceanic waters [45]. The same IOP spectra used in the HydroLight simulations were also used to calculate the $R_{rs}(\lambda)$ spectrum with the analytical models
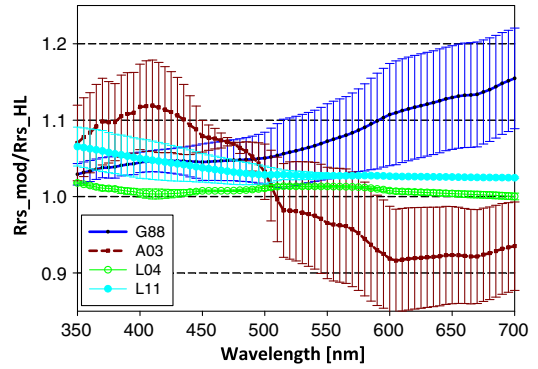

Fig. 3. Performance of analytical R_{rs} expressions in modeling hyperspectral $R_{rs}(\lambda)$. G88: Gordon *et al.* [19]; A03: Albert and Mobley [38]; L04: Lee *et al.* [36]; L11: Lee *et al.* [42].

[Eqs. (1), (2), (5), (6), and (8), respectively] for each [Chl] value. Then, the ratio of the analytically modeled $R_{rs}(\lambda)$ spectrum (Rrs_mod) to the Hydro-Light-simulated $R_{rs}(\lambda)$ spectrum (Rrs_HL) was calculated for each [Chl], along with the average and standard deviation of the ratios, respectively, of the five [Chl] for each analytical model. Figure 3 shows the results for the aforementioned four models. Generally, these ratios are within ±20%, consistent with the ranges presented in the articles for model development, but the four models do exhibit different behaviors. The ratio with the Gordon *et al.* [19] model (G88) shows a range of ~1.03–1.15 and generally increases with wavelength; and the ratio has a larger standard deviation for the longer wavelengths. The ratio of the Albert and Mobley [38] model (A03) spans a range of ~1.1 (shorter wavelength) to ~0.9 (longer wavelength), with a wide range of deviations for each wavelength, indicating a nonuniform performance for the [Chl] and wavelength. The ratio with the Lee *et al.* [36] model (L04) shows a range of ~1.0–1.02 for the entire 350–700-nm range and very small deviation across the spectral range. The ratio with the Lee *et al.* [42] model (L11) shows a range of ~1.03–1.07 and decreases with increasing wavelength. Models A03, L04, and L11 were developed based on numerical simulations by HydroLight, where a consistency between the model and HydroLight simulations is expected. Model G88 was developed based on Monte Carlo simulations, so there is a slight difference due to numerical handling of the radiative transfer [46] and the particle scattering phase functions used. Nevertheless, because models such as Eq. (6) provide a uniform performance for different chlorophyll concentrations and wavelengths, Model L04 is used in the following for the inversion of the IOPs.

B. Correction of Contribution due to Raman Scattering

The aforementioned analytical models [Eqs. (1), (5), (6), and (8)] reflect the processes resulting from elastic scattering—i.e., where there is no change of wavelength between the incident and output photons. In the oceans, inelastic scattering processes also

contribute photons to $R_{\mathrm{rs}}(\lambda)$, and Raman scattering is one of the inelastic scattering processes that can account for ~20% of the signal for oligotrophic waters in the long wavelengths [47–50]. Therefore, it is necessary to correct this effect in the measured $R_{\mathrm{rs}}(\lambda)$ spectrum for accurate derivation of the IOPs.

From the radiative transfer equation, it is found that the contribution to $R_{\mathrm{rs}}(\lambda)$ from Raman scattering can be written as [51,52]

$$R_{\mathrm{rs}}^{\mathrm{Ra}}(\lambda)$$
$$= \frac{(1-\rho_L)(1-\rho_E)}{n^2} \frac{b_{bw}^{\mathrm{Ra}}(\lambda_{ex})}{K_d(\lambda_{ex})+k_L(\lambda)} \frac{E_d(0+,\lambda_{ex})}{E_d(0+,\lambda)}(1+\delta). \tag{9}$$

Here, ρ_L and ρ_E are the air–sea surface reflectance for upwelling radiance and downwelling irradiance, respectively; n is the refractive index of seawater and is considered to be spectrally independent, $b_{bw}^{\mathrm{Ra}}(\lambda_{ex})$ is the Raman backscattering coefficient of pure seawater; K_d and k_L are the diffuse attenuation coefficients (m^{-1}) of downwelling irradiance and upwelling radiance, respectively; and $E_d(0+)$ is the downwelling irradiance just above the surface, where λ_{ex} is the excitation wavelength corresponding to λ. Parameter δ represents the secondary effects due to multiple scattering.

The wavelength gap between λ_{ex} and λ is ~40–140 nm for λ in the range of 350–700 nm ($\lambda > \lambda_{ex}$). Therefore, it is necessary to have K_d and $E_d(0+)$ information in the domain of ~310–350 nm to estimate $R_{\mathrm{rs}}^{Ra}(\lambda)$ for λ in the 350–400-nm range based on Eq. (9). The shortest wavelength of the radiance and irradiance measurements was approximately 350 nm (see Section 3), which prevented us from using Eq. (9) to analytically estimate $R_{\mathrm{rs}}^{Ra}(\lambda)$. To overcome this limitation in our data sets, we followed the empirical scheme as shown in Lee *et al.* [15,53] for the correction of Raman scattering. Basically, the no-Raman $R_{\mathrm{rs}}(\lambda)$ is expressed as

$$R_{\mathrm{rs}}(\lambda) = \frac{R_{\mathrm{rs}}^{T}(\lambda)}{1+\mathrm{RF}(\lambda)}. \tag{10}$$

Here, $R_{\mathrm{rs}}^{T}(\lambda)$ is the measured remote sensing reflectance that includes the contribution from Raman scattering, and RF is the Raman factor. Based on a series of numerical simulations with HydroLight for hyperspectral remote sensing reflectance, the empirical formula for $\mathrm{RF}(\lambda)$ is updated as

$$\mathrm{RF}(\lambda) = \alpha(\lambda)\left(\frac{R_{\mathrm{rs}}^{T}(440)}{R_{\mathrm{rs}}^{T}(550)}\right)^{\beta(\lambda)} + \gamma(\lambda)e^{-R_{\mathrm{rs}}^{T}(550)}, \tag{11}$$

with values for α, β, and γ for wavelengths in the range of 350–700 nm derived by fitting Eq. (11) to the RF values obtained from HydroLight simulations. $\mathrm{RF}(\lambda)$ is sensitive to the bandwidth of radiometers, as there are stronger relative effects caused by

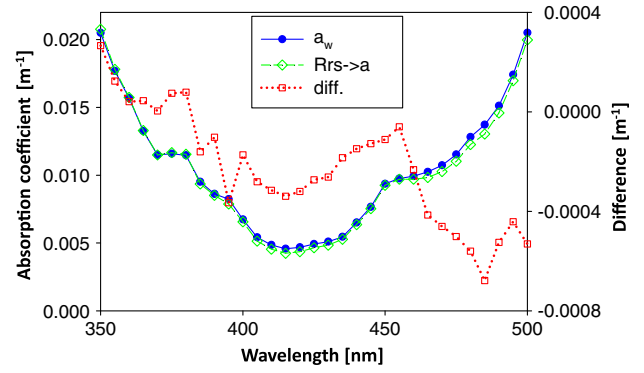
Fig. 4. Comparison between $a_w^{\mathrm{SPF}}(\lambda)$ (blue line) and inverted $a(\lambda)$ (green line) from HydroLight-simulated $R_{\mathrm{rs}}(\lambda)$ of pure seawater by QAA. Because there were no other components used in the Hydro-Light simulations, $a_w^{\mathrm{SPF}}(\lambda)$ is also the total absorption coefficient. HydroLight simulation included Raman scattering; this was corrected according to Eqs. (10) and (11). Red line (right axis) represents the difference $[a(\lambda) - a_w^{\mathrm{SPF}}(\lambda)]$.

the filling of the Fraunhofer lines [33]. Thus, two sets of α, β, and γ values were determined via this scheme—one for a bandwidth of 5 nm used for processing R_{rs} data measured at MOBY and another for a bandwidth of 10 nm used for the processing of R_{rs} measured in the South Pacific Gyre.

Other inelastic scattering processes, such as the gelbstoff fluorescence [54] and the chlorophyll-a fluorescence [55], also contribute to the measured upwelling radiance. Because the wavelength range in this study is outside the chlorophyll fluorescence band (~680 nm with a ~20 nm bandwidth) [55] and the contribution from gelbstoff fluorescence is negligible for such waters [56], it is appropriate to omit the contributions from these two sources for the studies herein.

C. Derivation of Total Absorption Coefficient

As discussed in detail in Lee *et al.* [20] regarding the QAA scheme, there are just two unknowns for any given $R_{\mathrm{rs}}(\lambda)$: $a(\lambda)$ and $b_b(\lambda)$. Therefore, $b_b(\lambda)$ can be analytically calculated if $a(\lambda)$ is known and vice versa. QAA starts the derivation process at a reference wavelength (λ_0), which is selected as 550 nm, and $a(550)$ is estimated following QAA (version 5; http://www.ioccg.org/groups/software.html). At this step, it is assumed that the values of $a_w^{\mathrm{SPF}}(\lambda)$ for $\lambda \geq 550$ nm are reliable, and $a_w^{\mathrm{SPF}}(550)$ was used for the estimation of $a(550)$. Further, instead of the "standard" QAA procedure for the calculation of $b_{bp}(550)$, where Eq. (1) is used to link r_{rs} with the IOPs, here $b_{bp}(550)$ is derived numerically based on Eq. (6) (i.e., Model L04) with $r_{\mathrm{rs}}(550)$ and $a(550)$ as inputs. $b_{bp}(550)$ is then extrapolated to the shorter wavelengths following Eq. (4) with $Y = 1.9$, a number based on the b_{bp} measurements presented in Huot *et al.* [28]. With $r_{\mathrm{rs}}(\lambda)$ and $b_{bp}(\lambda)$ known for the 350–550-nm range, the $a(\lambda)$ of each wavelength in this range is then derived by solving Eq. (6) again. In this process, the $b_{bw}(\lambda)$ values based
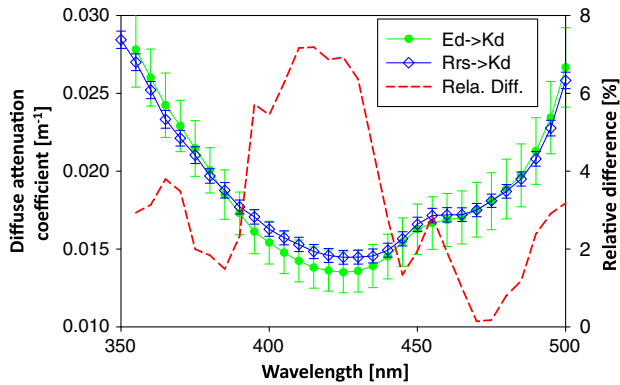
Fig. 5. Comparison between $K_d(\lambda)$ derived from $R_{\mathrm{rs}}(\lambda)$ and $K_d(\lambda)$ derived from the vertical profiles of $E_d(\lambda)$ for the "clearest" stations. Also shown (red line) is the spectrum of the relative difference between the two $K_d(\lambda)$.
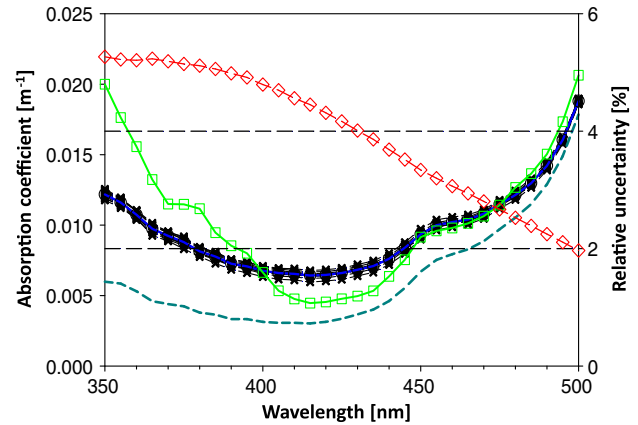

Fig. 6. Results of $a(\lambda)$ (black–blue lines) analytically derived from $R_{\mathrm{rs}}(\lambda)$ measured at the South Pacific Gyre, along with its relative uncertainty (red line, right axis) from algorithm error and $R_{\mathrm{rs}}(\lambda)$ measurement error. Also shown is $a_w^{\mathrm{SPF}}(\lambda)$ (green line) from Pope and Fry [4] (380–500 nm) and Sogandares and Fry [7] (350–375 nm, linearly interpolated to every 5 nm) and the baseline $a_w^B(\lambda)$ (the cyan line) derived from the $a(\lambda)$.

on Zhang et al. [25] with salinity as 38.4% for pure seawater were used.

To test the performance of this retrieval process, we first applied the scheme to the HydroLight-simulated $R_{\mathrm{rs}}(\lambda)$ of pure seawater [the green line in Fig. 2(a) with Raman scattering included; the values of $a_w^{\mathrm{SPF}}(\lambda)$ were used as the pure water absorption coefficient]. Figure 4 compares the QAA-retrieved $a(\lambda)$ with $a_w^{\mathrm{SPF}}(\lambda)$ (which is the total absorption coefficient of this case). The derived $a(\lambda)$ closely match $a_w^{\mathrm{SPF}}(\lambda)$ with a difference generally smaller than ~0.0004 m^{-1} (the red line in Fig. 4), indicating reliable retrievals of $a(\lambda)$ via the QAA scheme for such extreme waters. The slight difference between the two absorption spectra is due to simplifications of the radiative transfer [e.g., Eq. (6)] and the empirical handling of Raman contributions.

Further, the derived $a(420)$ from $R_{\mathrm{rs}}(\lambda)$ measurements made during BIOSOPE was compared with that derived from the combination of $K_d(420)$ and $R(420)$ (irradiance reflectance, which is the ratio of upwelling irradiance to downwelling irradiance just below the surface)—values derived from measurements of the vertical profiles of downwelling and upwelling irradiance [9]. Although the two approaches are completely different, along with different quantities used as inputs, the derived $a(420)$ values are very consistent (refer to a similar comparison in Lee et al. [15]), with $a(420)$ from $R_{\mathrm{rs}}(\lambda)$ slightly lower (~0.001 m^{-1}) than that from $K_d(420)$. Because there is no full spectral $a(\lambda)$ in Morel et al. [9] to evaluate the performance at other wavelengths, we instead compared the spectrum of $K_d(\lambda)$ of these "clearest" waters with the results presented in Fig. 5. This is because, generally, $a(\lambda)$ contributes 80% or more to $K_d(\lambda)$ [57,58]. Here, one $K_d(\lambda)$ represents the diffuse attenuation coefficient derived from vertical profiles of downwelling irradiance, while the other $K_d(\lambda)$ represents that estimated from $a(\lambda)$ and $b_b(\lambda)$ following the semi-analytical model developed in Lee et al. [53,58], with both $a(\lambda)$ and $b_b(\lambda)$ derived from $R_{\mathrm{rs}}(\lambda)$.

The comparison between the averaged $K_d(\lambda)$ (along with standard deviation) from vertical profiles and the averaged $K_d(\lambda)$ (and standard deviation) from $R_{\mathrm{rs}}(\lambda)$ for the "clearest" waters (Stations GYR2-5 and STB6-8) is presented in Fig. 5. The coefficient of determination (R^2) between the two averaged $K_d(\lambda)$ spectra is 0.996 ($N = 30$). The relative difference between the two values of $K_d(\lambda)$—calculated as $2 \times |K_{d1} - K_{d2}|/(K_{d1} + K_{d2})$—spans a range of ~1–7% for the 355–500-nm range, and the average over the wavelength range is ~3.4%. These results indicate very consistent determinations of $K_d(\lambda)$ from two independent methods for these "clearest" waters, although it is difficult to know which one is closer to the "truth," as each scheme has its own uncertainties. For instance, the slightly larger (~7%) difference for wavelengths around 420 nm [also the wavelengths with the lowest $K_d(\lambda)$] might be partially due to not correcting for Raman scattering in deriving $K_d(\lambda)$ from the vertical profiles of downwelling irradiance, which can lower the apparent attenuation of downwelling irradiance from this extra light "source" [44]. Because $a(\lambda)$ makes a large contribution to $K_d(\lambda)$, these results—along with the comparison of $a(420)$ and retrievals of $a(\lambda)$ from simulated pure water $R_{\mathrm{rs}}(\lambda)$—provide a confidence measure on the $a(\lambda)$ derived from the $R_{\mathrm{rs}}(\lambda)$ via QAA for such oligotrophic waters.

Figure 6 shows the 12 derived $a(\lambda)$ from the 12 R_{rs} spectra in super-blue waters [where $R_{\mathrm{rs}}(440)/R_{\mathrm{rs}}(550) > 12.0$] measured at the South Pacific Gyre; values for the 500–550-nm range are omitted in this figure to highlight the low absorption coefficients in the 350–500-nm range. The values generally vary in a range ~0.007 − 0.019 m^{-1} for wavelengths of 350–500 nm and are very consistent among each other (less than a ±5% variation). In addition, following the error propagation scheme [59], the uncertainty

in the derived $a(\lambda)$ due to potential errors of the QAA scheme is just ~2–5% for the 350–500-nm range (the red line in Fig. [6]), which suggests high confidence in the derived $a(\lambda)$. Such high precision in the derived $a(\lambda)$ is due to (1) very consistent (<2% uncertainty) measurements of $R_{rs}(\lambda)$ for such waters; and (2) the relatively large role played by molecular scattering. For instance, at 440 nm, $b_{bw}(440)$ makes ~67% of the total backscattering coefficient. Thus, even a 20% error in the estimation of $b_{bp}(440)$ will only result in a ~6% error in the estimated $a(440)$. However, because $a(550)$, where the value of $a_w^{SPF}(550)$ is considered as the true value, can be nearly precisely estimated for such waters, the error in the estimated $b_{bp}(440)$ is less than 5% [mainly due to uncertainty in $R_{rs}(550)$ and Eqs. ([6]) and ([7])] based on the error propagation theory. Further, only two assumptions—$a(550)$ and the $b_{bp}(\lambda)$ spectral dependence—are used in the derivation of $a(\lambda)$ from $R_{rs}(\lambda)$ via QAA, which ensures high accuracy and reliability of the analytically derived $a(\lambda)$ spectrum.

Also shown in Fig. [6] is $a_w^{SPF}(\lambda)$. The $a_w^{SPF}(\lambda)$ values are larger than the derived $a(\lambda)$ for the ~350- to 400-nm range and are smaller (~0.003 m^{-1}) than $a(\lambda)$ for wavelengths around 420 nm; there is almost no difference between $a_w^{SPF}(\lambda)$ and $a(\lambda)$ for wavelengths longer than 450 nm. Measurements from water samples (a_{ph}, a_y) indicate that the contribution from the optically active components is ~0.003 m^{-1} for 440 nm. This comparison explains the lack of closure of R_{rs} in Fig. [1] and the conclusion in Morel *et al.* [9] that the $a_w^{SPF}(\lambda)$ values are likely still too high for the 350–450-nm range for "pure" seawater. This further demonstrates the necessity to update this basic IOP for ocean optics and ocean color remote sensing.

To achieve this, we first derived an $a_w(\lambda)$ baseline [$a_w^B(\lambda)$] from the analytically inverted $a(\lambda)$ as

$$a_w^B(\lambda) = \bar{a}(\lambda) - a_{ph}(\lambda) - a_d(\lambda) - a_y(\lambda), \qquad (12)$$

where $\bar{a}(\lambda)$ is the average of the 12 $a(\lambda)$ spectra. Values of $a_{ph,d,y}(\lambda)$ were taken as the average of the lowest values of the gyre waters, as discussed in Section [2]. This $a_w^B(\lambda)$ (the cyan line in Fig. [6]) is not proposed as the "pure" seawater absorption coefficient, however, because the $R_{rs}(\lambda)$ during BIOSOPE was measured with a spectroradiometer (Satlantic, Inc.) with a 10-nm bandwidth. Thus, some details of the spectral curvature of pure seawater $a_w(\lambda)$ could not be revealed. This $a_w^B(\lambda)$ is, rather, applied further to the hyperspectral data collected at the MOBY site for the derivation of pure seawater $a_w(\lambda)$.

D. Derivation of Pure Seawater Absorption Coefficient

Using the $R_{rs}(\lambda)$ obtained at the MOBY site as input, $a(\lambda)$ was derived in the same way as presented in Section [4.C], except the Y value in Eq. [4(c)] was set
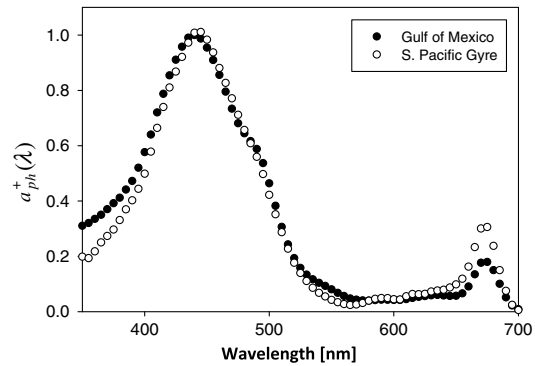

Fig. 7. Spectral shapes of phytoplankton absorption coefficient used for the derivation process.

as 1.0, following the results presented in Gordon *et al.* [60].

Unfortunately, there were no concurrent measurements of the component absorption coefficients (i.e., $a_{ph,d,y}$) that could be used; thus, the contributions of the optically active components had to be derived from $a(\lambda)$. Following widely adopted practices [27,61–63], the total absorption coefficient is expressed as

$$a(\lambda) = a_w^B(\lambda) + a_{ph}(\lambda) + a_{dy}(\lambda). \qquad (13)$$

Here, $a_{dy}(\lambda)$ represents the sum of a_d and a_y and is also expressed as an exponential function as Eq. [4(b)]

$$a_{dy}(\lambda) = a_{dy}(440)e^{-S_{dy}(\lambda-440)}. \qquad (14)$$

$a_{ph}(\lambda)$ was modeled following Eq. [4(a)], but two $a_{ph}^+(\lambda)$ shapes (shown in Fig. [7]) were used separately to ensure general representation. One $a_{ph}^+(\lambda)$ was measured at the South Pacific Gyre, while the other is from measurements made during various field experiments; these were limited to an $a_{ph}(440)$ of less than 0.02 m^{-1} (equivalent to [Chl] < 0.3 mg/m^3). Therefore, there are three unknowns for Eq. ([13]): $a_{ph}(440)$, $a_{dy}(440)$, and S_{dy}, and these unknowns
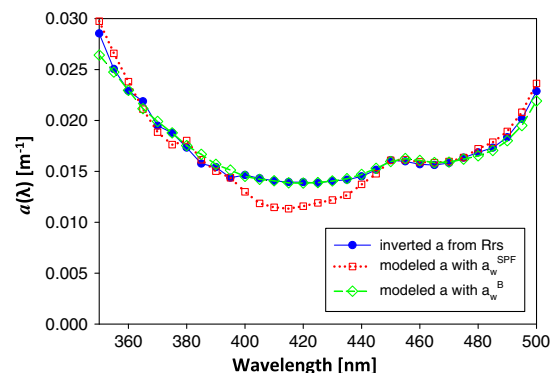

Fig. 8. Examples of $a(\lambda)$ when optimization is reached: one (red line) used the $a_w^{SPF}(\lambda)$ spectrum to model $a(\lambda)$, another (green line) used $a_w^B(\lambda)$; the blue line is the $a^T(\lambda)$ that was analytically inverted from $R_{rs}(\lambda)$.
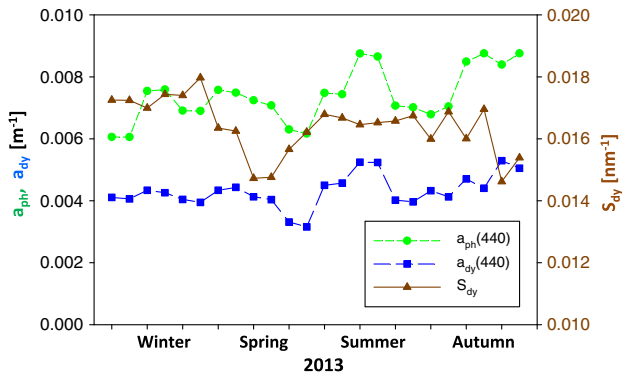
Fig. 9. Time series of $a_{\mathrm{ph}}(440)$, $a_{dy}(440)$, and S_{dy} of the MOBY water derived from $a(\lambda)$ through spectral optimization.

were derived by minimizing the following error function:

$$\mathrm{Err}^a = \frac{\sum_\lambda |a^T(\lambda) - a^M(\lambda)|}{\sum_\lambda a^T(\lambda)}, \qquad (15)$$

i.e., through a spectral optimization between the target $a^T(\lambda)$ and the modeled $a^M(\lambda)$. Here, $a^T(\lambda)$ is the spectrum analytically derived from $R_{\mathrm{rs}}(\lambda)$, while $a^M(\lambda)$ is that modeled via Eq. (13), and the wavelength range is 350–500 nm, a range in which the optically active components still make relatively large contributions. Figure 8 shows an example of the $a(\lambda)$ spectra when optimization is achieved. Generally, Err^a was approximately 2% when $a_w^B(\lambda)$ was used to model $a(\lambda)$, but it was approximately 5% when $a_w^{\mathrm{SPF}}(\lambda)$ was used. Using the $a_w^{\mathrm{SPF}}(\lambda)$, it was not possible to fit the 400–440-nm region well. This difference in Err^a provides additional support to the conclusion that values of $a_w^{\mathrm{SPF}}(\lambda)$ in the 350- to 500-nm range need to be revised.

After the component IOPs were derived, the absorption spectrum of "pure" seawater for λ in the range of 350–550 nm was derived [termed $a_w^D(\lambda)$ in the following] from each $a(\lambda)$ as

$$a_w^D(\lambda) = a(\lambda) - a_{\mathrm{ph}}(\lambda) - a_{dy}(\lambda). \qquad (16)$$

The final absorption spectrum of "pure" seawater is an average of the independently obtained $a_w^D(\lambda)$.

The derived seasonal $a_{\mathrm{ph}}(440)$, $a_{dy}(440)$, and S_{dy} are presented in Fig. 9, with $a_{\mathrm{ph}}(440)$ in the range of ~0.006–0.009 m^{-1}. This $a_{\mathrm{ph}}(440)$ range is equivalent to a [Chl] range of ~0.05–0.10 mg/m^3, following the bio-optical relationship developed by Bricaud et al. [64], which is generally consistent with the [Chl] value of those waters [60] and the range derived from the MODIS sensor. The derived $a_{dy}(440)$ is in the range of ~0.003–0.005 m^{-1}, with S_{dy} in the range of ~0.014–0.017 nm^{-1}—both generally consistent with sample observations in oligotrophic oceans [65,66]. In addition, from the vertical profiles of upwelling and downwelling irradiance measured at the MOBY site in February–March 2007, Gordon et al. [60] found that $a(443)$ was ~0.015 m^{-1}, a value consistent with that derived from $R_{\mathrm{rs}}(\lambda)$ (refer to Fig. 8). Further, without correcting the contribution of Raman scattering, Gordon et al. [60] obtained $b_b(462)$ as 0.0028 m^{-1}, which is consistent with a value of 0.0027 m^{-1} for $b_b(460)$ derived from $R_{\mathrm{rs}}(\lambda)$ via QAA if the Raman correction is omitted (not shown). These results regarding the total and component IOPs thus provide a validation of the analytical inversion of the total absorption and backscattering coefficients via QAA and the derivation of $a_{\mathrm{ph}}(\lambda)$ and $a_{dy}(\lambda)$ through spectral optimization, which then further validate the estimation of $a_w(\lambda)$.

5. Results and Discussion

Figure 10 shows the average (green diamond symbol) of $a_w^D(\lambda)$, along with a few $a_w(\lambda)$ spectra found in the literature and utilized in various eras. Also included in Fig. 10(b) (and Table 1) is the estimated uncertainty of $a_w^D(\lambda)$, which is derived from the absorption properties of the gyre waters following the error propagation scheme [67,68], which can be expressed as
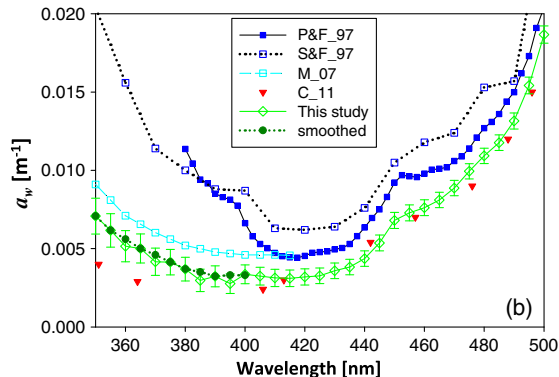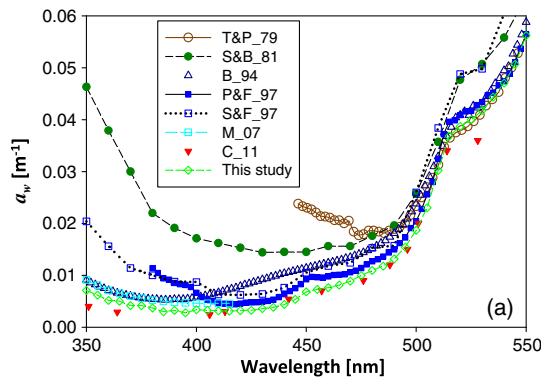

Fig. 10. $a_w^D(\lambda)$ and uncertainty (dark green) spectrum, along with a few $a_w(\lambda)$ spectra found in the literature (a) for wavelengths in the range of 350–550 nm and (b) zooming in on the range of 350–500 nm. T&P_79: Tam and Patel [6]; S&B_81: Smith and Baker [3]; B_94: Buiteveld [29]; P&F_97: Pope and Fry [4]; S&F_97: Sogandares and Fry [7]; M_07: Morel et al. [9]; C_11: Cruz et al. [69]. Spectra T&P_79, S&B_81, and B_94 were omitted in (b) for clarity.

Table 1. Derived Absorption Coefficient of "Pure" Seawater along with Uncertainties (Δa_w)[a]

Wavelength (nm)	a_w (m^{-1})	Smoothed a_w (m^{-1})	Δa_w (m^{-1})	Wavelength (nm)	a_w (m^{-1})	Δa_w (m^{-1})
350	0.0071	—	0.0011	455	0.0073	0.0005
355	0.0062	—	0.0011	460	0.0076	0.0005
360	0.0052	0.0056	0.0010	465	0.0081	0.0005
365	0.0050	—	0.0009	470	0.0089	0.0005
370	0.0042	0.0046	0.0009	475	0.0099	0.0005
375	0.0041	—	0.0008	480	0.0109	0.0005
380	0.0037	—	0.0008	485	0.0118	0.0005
385	0.0030	0.0035	0.0007	490	0.0132	0.0005
390	0.0032	—	0.0007	495	0.0154	0.0005
395	0.0028	0.0032	0.0006	500	0.0187	0.0005
400	0.0034	0.0032	0.0006	505	0.0230	0.0006
405	0.0032	—	0.0006	510	0.0302	0.0006
410	0.0031	—	0.0005	515	0.0368	0.0007
415	0.0031	—	0.0005	520	0.0387	0.0007
420	0.0032	—	0.0005	525	0.0400	0.0008
425	0.0033	—	0.0005	530	0.0418	0.0008
430	0.0036	—	0.0005	535	0.0443	0.0008
435	0.0038	—	0.0005	540	0.0470	0.0007
440	0.0044	—	0.0005	545	0.0507	0.0006
445	0.0054	—	0.0005	550	0.0562	0.0006
450	0.0068	—	0.0005	—	—	—

$$\Delta a_w(\lambda)$$
$$= \sqrt{(\Delta\bar{a}(\lambda))^2 + (\Delta a_{\mathrm{ph}}(\lambda))^2 + (\Delta a_d(\lambda))^2 + (\Delta a_y(\lambda))^2},$$

$$(17)$$

where $\Delta\bar{a}(\lambda)$, $\Delta a_{\mathrm{ph}}(\lambda)$, $\Delta a_d(\lambda)$, and $\Delta a_y(\lambda)$ are the uncertainties of each individual component, respectively. $\Delta\bar{a}(\lambda)$ was obtained following the QAA scheme, as discussed in Section 4.C, while the uncertainty of the component IOPs was estimated by assuming a 15% uncertainty [16] for each component. This $\Delta a_w(\lambda)$ is generally found to be approximately 0.0007 m^{-1} (~1–20%) for the 350–550-nm range, suggesting high precision in the derived absorption coefficient of "pure" seawater.

Because the difference between $a_w^D(\lambda)$ and $a_w^{\mathrm{SPF}}(\lambda)$ for the 500–550-nm range is small (~1–10%), the following discussions will focus on the 350–500-nm range. However, from 510 to 550 nm, the $a_w^D(\lambda)$ follow very closely (the difference is <0.001 m^{-1} or <4%) to the measurements of Tam and Patel [6], which are also lower than $a_w^{\mathrm{SPF}}(\lambda)$ in this spectral region. For the 420–500-nm range, the values of $a_w^D(\lambda)$ have almost exactly the same spectral shape ($R^2 = 0.996$, $N = 17$) as that of $a_w^{\mathrm{SPF}}(\lambda)$, including a shoulder around 450 nm, but the $a_w^D(\lambda)$ values are slightly lower (~0.002 m^{-1}) than the values of $a_w^{\mathrm{SPF}}(\lambda)$. For the 350–415-nm range, however, $a_w^D(\lambda)$ do not have the same spectral shape as that of $a_w^{\mathrm{SPF}}(\lambda)$ ($R^2 = 0.871$, $N = 14$), and the $a_w^D(\lambda)$ values are smaller than $a_w^{\mathrm{SPF}}(\lambda)$ by approximately a factor of 2. Most importantly, as opposed to that shown in Pope and Fry [4] and Sogandares and Fry [7], the values of $a_w^D(\lambda)$ do not increase significantly as the

wavelength decreases. However, for this spectral range, $a_w^D(\lambda)$ show a very similar spectral shape ($R^2 = 0.974$, $N = 14$) to $a_w^{\mathrm{MPF}}(\lambda)$, although the $a_w^D(\lambda)$ values are lower by approximately 0.002 m^{-1}. Recently, Cruz et al. [69], with a thermal lens spectrometry technique, measured the pure water absorption coefficient at discrete wavelengths; these are also presented in Fig. 10. Interestingly, for the 410–510-nm range, the values of $a_w^D(\lambda)$ and $a_w(\lambda)$ of Cruz et al. [69] are nearly identical (<5% difference), although the $a_w(\lambda)$ values of Cruz et al. [69] are slightly lower than the values of $a_w^D(\lambda)$ for wavelengths shorter than ~405 nm.

There are four tiny dips in $a_w^D(\lambda)$ for the 350- to 400-nm range, which are likely a result of an imperfect removal of the Raman contributions in the measured $R_{\mathrm{rs}}(\lambda)$ [refer to Fig. 2(b)]. We smoothed these dips by a simple average between the shoulders, with the results shown as the green dotted line in Fig. 10(b). These results are also included in Table 1.

The ~0.002 m^{-1} lower value of $a_w^D(\lambda)$ compared to that of $a_w^{\mathrm{SPF}}(\lambda)$ for the 420–500 nm range is within the uncertainty between Pope and Fry [4] and Sogandares and Fry [7]; they are also, generally, within two standard deviations of the measurements as reported by Pope and Fry [4]. Such differences and uncertainties indicate the difficulties in accurately measuring such small values in the laboratory. This is particularly true for the wavelength range of 350–415 nm, where $a_w(\lambda)$ values are approximately or less than 0.005 m^{-1}, which indicates a loss of just 0.5% of the optical signal due to absorption for a 1-m cuvette. For measured $R_{\mathrm{rs}}(\lambda)$ in the field, however, 90% of the measured signal comes from the first attenuation
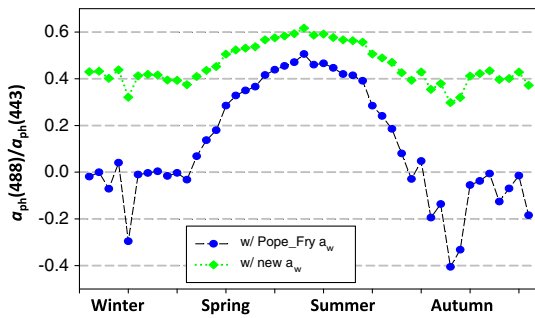
Fig. 11. Ratio of $a_{\mathrm{ph}}(488)$ to $a_{\mathrm{ph}}(443)$ derived from climatological $R_{\mathrm{rs}}(\lambda)$ collected at the South Pacific Gyre for a region (140–130°W, 23–28°S) by MODIS Aqua.

depth [70]. Because the attenuation coefficients of such waters are $\sim$0.015–0.025 m^{-1} for this spectral range (refer to Fig. 5), this indicates that the measured radiance originates from a layer deeper than $\sim$40 m. Measurements of optical interactions over such long path lengths provide orders of magnitude stronger signal than many laboratory settings for such waters (the path length of the integrating sphere approach taken by Pope and Fry [4] can be a few meters for pure waters). Thus, more accurate results can be expected. On the downside of such determinations is the need for sophisticated models to interpret them and sufficient knowledge of the "contaminating" IOPs. The lower $a_w^D(\lambda)$ compared to $a_w^{\mathrm{MPF}}(\lambda)$ [9] for the 350–415-nm range, however, is consistent with the conclusion in Morel *et al.* [9] that the combination of Boivin *et al.* [30] and Pope and Fry [4] values works as an upper limit of the absorption coefficient of pure seawater.

There is no "standard" to validate the $a_w^D(\lambda)$ values, apart from the fact that they must not be negative and should be consistent in general with values in the literature for wavelengths in the range of 350–550 nm (refer to Fig. 10). An indirect validation of this new $a_w(\lambda)$ is its application to the MODIS climatological times series over the South Pacific Gyre (140–130° W, 23–28° N), where MODIS $R_{\mathrm{rs}}(\lambda)$ was used to retrieve $a_{\mathrm{ph}}(\lambda)$ using QAA (with the default scheme for the estimation of S_{dy}) for bands with center wavelengths at 443 and 488 nm. Further, the ratio $a_{\mathrm{ph}}(488)/a_{\mathrm{ph}}(443)$ was calculated, where there is no assumption about the value of this ratio in the QAA derivation process. For oligotrophic waters with low [Chl], sample measurements indicate that this ratio is approximately 0.5 and very stable [64,71]. However, when $a_w^{\mathrm{SPF}}(\lambda)$ values were used, a wide and strange range of $a_{\mathrm{ph}}(488)/a_{\mathrm{ph}}(443)$ values resulted (Fig. 11, blue line), and many times the independently derived $a_{\mathrm{ph}}(488)$ became negative. Although the inversion algorithm is not perfect, it is difficult to explain the negative $a_{\mathrm{ph}}(488)$ derived from the MODIS $R_{\mathrm{rs}}(\lambda)$, which went through multiple layers of quality control (averaged over a large area and from multi-year observations, along with screening for observations with a large sensor viewing angle and sun angle, high sun glint, and heavy aerosol

load). In addition, the uncertainty in the derived $a(488)$ due to QAA is just about 2% for such waters (refer to Fig. 6). When the $a_w^{\mathrm{SPF}}(\lambda)$ values were replaced by $a_w^D(\lambda)$ with the same QAA process, however, the $a_{\mathrm{ph}}(488)/a_{\mathrm{ph}}(443)$ ratio changed to $\sim$0.4–0.6 (refer to the green line in Fig. 11)—values generally consistent with sample measurements of phytoplankton pigments. This significant change in the $a_{\mathrm{ph}}(488)/a_{\mathrm{ph}}(443)$ ratio that was independently derived from MODIS observations, at least partially, provides support for the fidelity of $a_w^D(\lambda)$ for "pure" seawater. At the very least, it shows internal consistency. The slight temporal variation of $a_{\mathrm{ph}}(488)/a_{\mathrm{ph}}(443)$ could be a result of an imperfect Raman correction for such climatological data and/or an imperfect estimation of S_{dy} used in QAA, which is beyond the scope of this research.

6. Conclusions

Based on hyperspectral measurements of remote sensing reflectance in the oligotrophic oceans and an accurate relationship between $R_{\mathrm{rs}}(\lambda)$ and the IOPs, and assuming that $a_w^{\mathrm{SPF}}(550)$ is correct, the spectra of the total absorption coefficient and the absorption coefficient of "pure" seawater were derived analytically (for the range of 350–550 nm). The derived $a_w(\lambda)$ shows values that are consistent (very similar shape) with those from Pope and Fry [4] for the range of 420–550 nm. They are reduced by $\sim$0.002 m^{-1} but nearly the same (differing by <0.001 m^{-1} or <4%) as those measured by Tam and Patel [6] for the 510–550-nm range and those of Cruz *et al.* [69] for the 410–510-nm range. For the 350–400-nm range, however, the derived $a_w(\lambda)$ values are considerably lower (by approximately a factor of 2) and do not have the same spectral shape as those reported in Pope and Fry [4] and Sogandares and Fry [7]; they are slightly higher ($\sim$0.002 m^{-1}) than those of Cruz *et al.* [69]. Initial tests with the new $a_w(\lambda)$ values resulted in retrievals of more realistic phytoplankton absorption spectral shapes from observations of $R_{\mathrm{rs}}(\lambda)$. Based on multiple consistent lines of evidence, these newly derived $a_w(\lambda)$ values appear to be closer to the true absorption coefficient of "pure" seawater than previous estimates.

suggestions from the two anonymous reviewers are greatly appreciated.

References

1. R. W. Preisendorfer, *Hydrologic Optics Vol. 1: Introduction* (National Technical Information Service, Office of Naval Research, 1976).
2. A. Morel and L. Prieur, "Analysis of variations in ocean color," Limnol. Oceanogr. **22**, 709–722 (1977).
3. R. C. Smith and K. S. Baker, "Optical properties of the clearest natural waters," Appl. Opt. **20**, 177–184 (1981).
4. R. Pope and E. Fry, "Absorption spectrum (380–700 nm) of pure water. II. Integrating cavity measurements," Appl. Opt. **36**, 8710–8723 (1997).
5. E. S. Fry, "Visible and near-ultraviolet absorption spectrum of liquid water: comment," Appl. Opt. **39**, 2743–2744 (2000).
6. A. C. Tam and C. K. N. Patel, "Optical absorptions of light and heavy water by laser optoacoustic spectroscopy," Appl. Opt. **18**, 3348–3358 (1979).
7. F. M. Sogandares and E. S. Fry, "Absorption spectrum (340–640 nm) of pure water. I. Photothermal measurements," Appl. Opt. **36**, 8699–8709 (1997).
8. Z. Lee, J. E. Ivey, K. L. Carder, R. G. Steward, and J. S. Patch, "Pure water absorption coefficient around 400 nm: lab measured versus field observed," in *Ocean Optics XV*, Monaco, Oct 16–20, 2000.
9. A. Morel, B. Gentili, H. Claustre, A. Babin, A. Bricaud, J. Ras, and F. Tieche, "Optical properties of the 'clearest' natural waters," Limnol. Oceanogr. **52**, 217–229 (2007).
10. A. Mannino, M. G. Novak, S. B. Hooker, K. Hyde, and D. Aurin, "Algorithm development and validation of CDOM properties for estuarine and continental shelf waters along the northeastern U.S. coast," Remote Sens. Environ. **152**, 576–602 (2014).
11. J. Wei and Z. P. Lee, "Retrieval of phytoplankton and CDM absorption coefficients in the ocean with remote sensing reflectance in an ultraviolet (UV) band," Appl. Opt. (in press).
12. H. R. Gordon and A. Morel, *Remote Assessment of Ocean Color for Interpretation of Satellite Visible Imagery: A Review* (Springer-Verlag, 1983).
13. J. R. V. Zaneveld, "A theoretical derivation of the dependence of the remotely sensed reflectance of the ocean on the inherent optical properties," J. Geophys. Res. **100**, 13135–13142 (1995).
14. H. Claustre, A. Sciandra, and D. Vaulot, "Introduction to the special section bio-optical and biogeochemical conditions in the South East Pacific in late 2004: the BIOSOPE program," Biogeosciences **5**, 679–691 (2008).
15. Z.-P. Lee, S. Shang, C. Hu, M. Lewis, R. Arnone, Y. Li, and B. Lubac, "Time series of bio-optical properties in a subtropical gyre: implications for the evaluation of inter-annual trends of biogeochemical properties," J. Geophys. Res. **115**, C09012 (2010).
16. A. Bricaud, M. Babin, H. Claustre, J. Ras, and F. Tieche, "Light absorption properties and absorption budget of Southeast Pacific waters," J. Geophys. Res. **115**, C08009 (2010).
17. M. S. Twardowski, H. Claustre, S. A. Freeman, D. Stramski, and Y. Huot, "Optical backscattering properties of the 'clearest' natural waters," Biogeosciences **4**, 1041–1058 (2007).
18. D. Stramski, R. A. Reynolds, M. Babin, S. Kaczmarek, M. R. Lewis, R. Röttgers, A. Sciandra, M. Stramska, M. S. Twardowski, B. A. Franz, and H. Claustre, "Relationships between the surface concentration of particulate organic carbon and optical properties in the eastern South Pacific and eastern Atlantic Oceans," Biogeosciences **5**, 171–201 (2008).
19. H. R. Gordon, O. B. Brown, R. H. Evans, J. W. Brown, R. C. Smith, K. S. Baker, and D. K. Clark, "A semianalytic radiance model of ocean color," J. Geophys. Res. **93**, 10909–10924 (1988).
20. Z. P. Lee, K. L. Carder, and R. Arnone, "Deriving inherent optical properties from water color: a multi-band quasi-analytical algorithm for optically deep waters," Appl. Opt. **41**, 5755–5772 (2002).
21. J. T. O. Kirk, *Light & Photosynthesis in Aquatic Ecosystems* (University, 1994).
22. C. D. Mobley, *Light and Water: Radiative Transfer in Natural Waters* (Academic, 1994).
23. W. S. Pegau, D. Gray, and J. R. V. Zaneveld, "Absorption and attenuation of visible and near-infrared light in water: dependence on temperature and salinity," Appl. Opt. **36**, 6035–6046 (1997).
24. J. M. Sullivan, M. S. Twardowski, J. R. V. Zaneveld, C. M. Moore, A. H. Barnard, P. L. Donaghay, and B. Rhoades, "Hyperspectral temperature and salt dependencies of absorption by water and heavy water in the 400-750 nm spectral range," Appl. Opt. **45**, 5294–5309 (2006).
25. X. Zhang, L. Hu, and M.-X. He, "Scattering by pure seawater: effect of salinity," Opt. Express **17**, 5698–5710 (2009).
26. R. A. Arnone, "Remote sensing of ocean colour in coastal, and other optically-complex, waters," Reports of the International Ocean-Colour Coordinating Group No. 3, S. Sathyendranath, ed. (IOCCG, 2000).
27. Z.-P. Lee, ed., "Remote sensing of inherent optical properties: fundamentals, tests of algorithms, and applications," Reports of the International Ocean-Colour Coordinating Group No. 5 (IOCCG, 2006).
28. Y. Huot, A. Morel, M. S. Twardowski, D. Stramski, and R. A. Reynolds, "Particle optical backscattering along a chlorophyll gradient in the upper layer of the eastern South Pacific Ocean," Biogeosciences **5**, 495–507 (2008).
29. H. Buiteveld, J. H. M. Hakvoort, and M. Donze, "The optical properties of pure water," Proc. SPIE **2258**, 174–183 (1994).
30. L. P. Boivin, W. F. Davidson, R. S. Storey, D. Sinclair, and E. D. Earle, "Determination of the attenuation coefficients of visible and ultraviolet radiation in heavy water," Appl. Opt. **25**, 877–882 (1986).
31. C. D. Mobley and L. K. Sundman, *HydroLight 5.2 User's Guide* (Sequoia Scientific, 2013).
32. D. K. Clark, H. R. Gordon, K. J. Voss, Y. Ge, W. Broenkow, and C. Trees, "Validation of atmospheric correction over the oceans," J. Geophys. Res. **102**, 17209–17217 (1997).
33. C. Hu and K. J. Voss, "In situ measurements of Raman scattering in clear ocean water," Appl. Opt. **36**, 6962–6967 (1997).
34. S. Sathyendranath and T. Platt, "Analytic model of ocean color," Appl. Opt. **36**, 2620–2629 (1997).
35. H. J. V. D. Woerd and R. Pasterkamp, "HYDROPT: a fast and flexible method to retrieve chlorophyll-a from multispectral satellite observations of optically complex coastal waters," Remote Sens. Environ. **112**, 1795–1807 (2008).
36. Z. P. Lee, K. L. Carder, and K. P. Du, "Effects of molecular and particle scatterings on model parameters for remote-sensing reflectance," Appl. Opt. **43**, 4957–4964 (2004).
37. Y.-J. Park and K. Ruddick, "Model of remote-sensing reflectance including bidirectional effects for case 1 and case 2 waters," Appl. Opt. **44**, 1236–1249 (2005).
38. A. Albert and C. D. Mobley, "An analytical model for subsurface irradiance and remote sensing reflectance in deep and shallow case-2 waters," Opt. Express **11**, 2873–2890 (2003).
39. A. Morel, "Optical properties of pure water and pure sea water," in *Optical Aspects of Oceanography*, N. G. Jerlov and E. S. Nielsen, eds. (Academic, 1974), pp. 1–24.
40. A. Morel and B. Gentili, "Diffuse reflectance of oceanic waters: its dependence on sun angle as influenced by the molecular scattering contribution," Appl. Opt. **30**, 4427–4438 (1991).
41. A. Morel and H. Loisel, "Apparent optical properties of oceanic water: dependence on the molecular scattering contribution," Appl. Opt. **37**, 4765–4776 (1998).
42. Z.-P. Lee, K. Du, K. J. Voss, G. Zibordi, B. Lubac, R. Arnone, and A. Weidemann, "An inherent-optical-property-centered approach to correct the angular effects in water-leaving radiance," Appl. Opt. **50**, 3155–3167 (2011).
43. A. Morel and B. Gentili, "Diffuse reflectance of oceanic waters (2): bi-directional aspects," Appl. Opt. **32**, 6864–6879 (1993).
44. A. Morel, D. Antoine, and B. Gentili, "Bidirectional reflectance of oceanic waters: accounting for Raman emission and varying particle scattering phase function," Appl. Opt. **41**, 6289–6306 (2002).

45. A. Morel and S. Maritorena, "Bio-optical properties of oceanic waters: a reappraisal," J. Geophys. Res. **106**, 7163–7180 (2001).

46. C. D. Mobley, B. Gentili, H. R. Gordon, Z. Jin, G. W. Kattawar, A. Morel, P. Reinersman, K. Stamnes, and R. H. Stavn, "Comparison of numerical models for computing underwater light fields," Appl. Opt. **32**, 7484–7504 (1993).

47. S. Sugihara, M. Kishino, and N. Okami, "Contribution of Raman scattering to upward irradiance in the sea," J. Oceanogr. Soc. Jpn. **40**, 397–404 (1984).

48. R. H. Stavn and A. D. Weidemann, "Optical modeling of clear ocean light fields: Raman scattering effects," Appl. Opt. **27**, 4002–4011 (1988).

49. B. R. Marshall and R. C. Smith, "Raman scattering and in-water ocean properties," Appl. Opt. **29**, 71–84 (1990).

50. H. R. Gordon, "Influence of Raman scattering on the light field in natural waters: a simple assessment," Opt. Express **22**, 3675–3683 (2014).

51. S. Sathyendranath and T. Platt, "Ocean-color model incorporating transspectral processes," Appl. Opt. **37**, 2216–2227 (1998).

52. T. K. Westberry, E. Boss, and Z. Lee, "The influence of Raman scattering on ocean color inversion models," Appl. Opt. **52**, 5552–5561 (2013).

53. Z. Lee, C. Hu, S. Shang, K. Du, M. Lewis, R. Arnone, and R. Brewin, "Penetration of UV-visible solar light in the global oceans: insights from ocean color remote sensing," J. Geophys. Res. **118**, 4241–4255 (2013).

54. S. K. Hawes, K. L. Carder, and G. R. Harvey, "Quantum fluorescence efficiencies of marine humic and fulvic acids: effects on ocean color and fluorometric detection," Proc. SPIE **1750**, 212 (1992).

55. H. R. Gordon, "Diffuse reflectance of the ocean: the theory of its augmentation by chlorophyll a fluorescence at 685 nm," Appl. Opt. **18**, 1161–1166 (1979).

56. Z. Lee, K. Carder, S. Hawes, R. Steward, T. Peacock, and C. Davis, "Model for interpretation of hyperspectral remote-sensing reflectance," Appl. Opt. **33**, 5721–5732 (1994).

57. H. R. Gordon, "Can the Lambert-Beer law be applied to the diffuse attenuation coefficient of ocean water?" Limnol. Oceanogr. **34**, 1389–1409 (1989).

58. Z. P. Lee, K. P. Du, and R. Arnone, "A model for the diffuse attenuation coefficient of downwelling irradiance," J. Geophys. Res. **110**, C02016 (2005).

59. Z.-P. Lee, R. Arnone, C. Hu, P. J. Werdell, and B. Lubac, "Uncertainties of optical parameters and their propagations in an analytical ocean color inversion algorithm," Appl. Opt. **49**, 369–381 (2010).

60. H. R. Gordon, M. R. Lewis, S. D. McLean, M. S. Twardowski, S. A. Freeman, K. J. Voss, and G. C. Boynton, "Spectra of particulate backscattering in natural waters," Opt. Express **17**, 16192–16208 (2009).

61. K. L. Carder, S. K. Hawes, K. A. Baker, R. C. Smith, R. G. Steward, and B. G. Mitchell, "Reflectance model for quantifying chlorophyll a in the presence of productivity degradation products," J. Geophys. Res. **96**, 20599–20611 (1991).

62. C. S. Roesler and M. J. Perry, "In situ phytoplankton absorption, fluorescence emission, and particulate backscattering spectra determined from reflectance," J. Geophys. Res. **100**, 13279–13294 (1995).

63. S. Maritorena, D. A. Siegel, and A. R. Peterson, "Optimization of a semianalytical ocean color model for global-scale applications," Appl. Opt. **41**, 2705–2714 (2002).

64. A. Bricaud, A. Morel, M. Babin, K. Allali, and H. Claustre, "Variations of light absorption by suspended particles with chlorophyll a concentration in oceanic (case 1) waters: analysis and implications for bio-optical models," J. Geophys. Res. **103**, 31033–31044 (1998).

65. N. Nelson, D. Siegel, and A. Michaels, "Seasonal dynamics of colored dissolved material in the Sargasso Sea," Deep Sea Res. **45**, 931–957 (1998).

66. M. S. Twardowski, E. Boss, J. M. Sullivan, and P. L. Donaghay, "Modeling the spectral shape of absorption by chromophoric dissolved organic matter," Mar. Chem. **89**, 69–88 (2004).

67. S. L. Meyer, *Data Analysis for Scientists and Engineers* (Wiley, 1975).

68. H. R. Gordon, "Radiometric considerations for ocean color remote sensors," Appl. Opt. **29**, 3228–3236 (1990).

69. R. A. Cruz, M. C. Filadelpho, M. P. P. Castro, A. A. Andrade, C. M. M. Souza, and T. Catunda, "Very low optical absorptions and analyte concentrations in water measured by optimized thermal lens spectrometry," Talanta **85**, 850–858 (2011).

70. H. R. Gordon and W. R. McCluney, "Estimation of the depth of sunlight penetration in the sea for remote sensing," Appl. Opt. **14**, 413–416 (1975).

71. A. Bricaud, M. Babin, A. Morel, and H. Claustre, "Variability in the chlorophyll-specific absorption coefficients of natural phytoplankton: analysis and parameterization," J. Geophys. Res. **100**, 13321–13332 (1995).